Vol. 33, No. 4 (2023) | DOI: 10.37190/ord230405

OPEN ACCESS

Operations Research and Decisions

www.ord.pwr.edu.pl

OPERATIONS RESEARCH AND DECISIONS QUARTERLY

Analysis of COVID-19 and cancer data using new half-logistic generated family of distributions

Sadaf Khan[1, 2*] Muhammad H. Tahir[1] Farrukh Jamal[1]

[1] *Department of Statistics, The Islamia University of Bahawalpur, Punjab, Pakistan*

[2] *Department of Social and Allied Sciences, Cholistan University of Veterinary and Animal Sciences, Bahawalpur, Punjab, Pakistan*

[*] *Corresponding author, email address: smkhan6022@gmail.com*

Abstract

We focus on a specific sub-model of the proposed family that we call the new half logistic-Fréchet. This sub-model stems from a new generalisation of the half-logistic distribution which we call the new half-logistic-G. The novelty of proposing this new family is that it does not include any additional parameters and instead relies on the baseline parameter. Standard statistical formulas are used to show the forms of the density and failure rate functions, ordinary and incomplete moments with generating functions, and random variate generation. The maximum likelihood estimation procedure is used to estimate the set of parameters. We conduct a simulation analysis to ensure that our calculations are converging with lower mean square error and biases. We use three real-life data sets to equate our model to well-established existing models. The proposed model outperforms the well-established four parameters beta Fréchet and exponentiated generalized Fréchet for some real--life results, with three parameters such as half-logistic Fréchet, exponentiated Fréchet, Zografos–Balakrishnan gamma Fréchet, Topp–Leonne Fréchet, and Marshall–Olkin Fréchet and two-parameter classical Fréchet distribution.

Keywords: *half-logistic distribution, generalized family, likelihood estimation, bio-medical data, Fréchet distribution*

1. Introduction

Modern distribution theory is still developing. Researchers often devise novel methods for generating univariate probability distributions. Regardless of how complex the model is, a distribution with the fewest possible parameters is generally preferred. The shift in approach is largely due to the introduction of digital computers (particularly automatic differentiation and numerical integration), new machine learning techniques, and the use of computer software such as Mathematica, Matlab, Python, and R-language to analyse large amounts of data. Furthermore, these methods have helped applied practitioners explore some of their unique models, which can be applied to a variety of fields, including reliability engineering, bioinformatics, hydrology, survival analysis, soil sciences, actuarial research, and others.

Received 22 December 2022, accepted 17 August 2023, published online 22 December 2023
ISSN 2391-6060 (Online)/© 2023 Authors

The costs of publishing this issue have been co-financed by the program *Development of Academic Journals* of the Polish Ministry of Education and Science under agreement RCN/SP/0241/2021/1

Tahir et al. [20] suggested a new family of distributions, such as new flexible G-family, abbreviated as NFGF for $T \in (0,1)$. For any baseline distribution with survival function (sf) as $\bar{D}(x;\varsigma)$ or distribution function (cdf) as $D(x;\varsigma)$ and density function (pdf) as $d(x;\varsigma)$, the new family's cdf and pdf are, respectively, denoted by

$$F(x;\varsigma) = 1 - \bar{D}(x;\varsigma)^{D(x;\varsigma)} \tag{1}$$

and

$$f(x;\varsigma) = d(x;\varsigma)\,\bar{D}(x;\varsigma)^{D(x;\varsigma)}\left(\frac{D(x;\varsigma)}{\bar{D}(x;\varsigma)} - \log\,\bar{D}(x;\varsigma)\right)$$

The authors pioneered a flexible cdf in (1), which acts as a substitute to extend several well-known G-classes of distribution. Some of the other existing prominent G-classes which were never deduced from a preceding parent model, namely Marshall–Olkin-G [15], exponential-G (EG) with Lehmann alternative of type-I (LA-1) [14] and Lehmann alternative of type-II (LA-2) [6], transmuted-G (TrG) [19] and cubic rank transmuted-G (CrTRG) [9] are also mentioned.

This inspired and encouraged us to introduce a new family of naturally occurring distributions. We propose a new generator $W[R(x)] = -\log[\bar{D}(x;\varsigma)]^{D(x;\varsigma)}$ with support over $\mathbb{R}+$ to generalise half-logistic distribution, i.e., *New Half Logistic-G* (NHLG for short)) class of distributions, based on the premises of [20]. Further motivations for introducing the NHLG family of distributions include:

- the NHLG is constituted without any additional parameters;
- the proposed family has not been developed by an existing parent model;
- the link function $W[R(x)]$ can be used further to develop other G-class with support $T \in (-\infty, +\infty)$;
- the model is annotated with the view that it will attract a wider class of applied statisticians due to its ability to significantly improve the quality of fit (GoFs) measures;
- the model offers greater flexibility and tractability in terms of its tail properties;
- various flexible shapes of pdf and hazard rate function (hf) can be extracted as a result of new special models arising from NHLG.

The paper is organized as follows. In Section 2, we proposed a unique generator NHLG. In Section 3, the mathematical foundation of the proposed generalization which includes distinctive special models from NHLG, linear representation of distribution function, analytical shapes of density and hazard rate, quantile function, moments and generating functions are established. Further, inference related to the model parameters is also derived with explicit expressions. The Fréchet distribution as baseline distribution to define the new half-logistic Fréchet (NHLFr) from the postulated NHLG family is studied with its properties in Section 3. Additionally, a simulation study has been conducted in order to show the convergence of the model parameter. Section 4 comprises some concluding remarks and future possibilities related to the defined model.

2. The proposed family

Let T follows half-logistic (HL) random variable (rv) with $r(t) = 2\mathrm{e}^{-\lambda t}(1+\mathrm{e}^{-\lambda t})^{-2}$ be the pdf and $R(t) = (1-\mathrm{e}^{-\lambda t})(1+\mathrm{e}^{-\lambda t})^{-1}$ be the cdf, with support $0 < \xi < \infty$. Let us say $K[D(x;\varsigma)]$ serves as the generator function of any baseline rv's cdf $R(t)$ so that $K[D(x;\varsigma)]$ meets the following criteria:

a) $K[D(x;\,\varsigma)] \in [\xi]$,

b) $K[D(x;\,\varsigma)]$ is uniformly non-decreasing and differentiable,

c) $K[D(x;\,\varsigma)] \to \xi$ as $x \to 0$ and $K[D(x;\,\varsigma)] \to \xi$ as $x \to +\infty$.

Then setting $K[D(x)] = -\log[\bar{D}(x;\,\varsigma)]^{D(x;\,\varsigma)}$ and using the conceptual framework referenced in [3] by Alzaatreh's et al., the cdf and pdf of NHLG family of distributions are defined as

$$F(x;\,\varsigma) = \int_{a}^{-\log\left(\{\bar{D}(x;\,\varsigma)\}^{D(x;\,\varsigma)}\right)} 2\lambda \mathrm{e}^{-\lambda t}\,\left(1+\mathrm{e}^{-\lambda t}\right)^{-2} dt = \frac{1-\bar{D}(x;\,\varsigma)^{\lambda\, D(x;\varsigma)}}{1+\bar{D}(x;\,\varsigma)^{\lambda\, D(x;\varsigma)}}, \quad x>0 \tag{2}$$

where $\lambda > 0$ acts as a shape parameter and ς is the vector of baseline parameter.

The pdf corresponding to (2) is given by

$$f(x;\,\varsigma) = \frac{2\lambda\, d(x;\,\varsigma)\bar{D}(x;\,\varsigma)^{\lambda\, D(x;\varsigma)-1}}{\left(1+\bar{D}(x;\,\varsigma)^{\lambda\, D(x;\varsigma)}\right)^2}\left(\{1+\log\bar{D}(x;\,\varsigma)\}D(x;\,\varsigma)-\log\bar{D}(x;\,\varsigma)\right) \tag{3}$$

where $\bar{D} = 1 - D(x;\,\varsigma)$ is the baseline sf and $d(x;\,\varsigma)$ is the baseline pdf. We can generate a new half-logistic generalized class of distributions for each baseline, sometimes, by ignoring the dependence on the vector ς of the parameters and simply write $D(x) = D(x;\,\varsigma)$ and $d(x) = d(x;\,\varsigma)$. Henceforth, $X \sim \text{NHLG}(\lambda,\,\varsigma)$ denotes a random variable having density (3).

The sf and the hf of X are, respectively, given by

$$\bar{F}(x) = \frac{2\,\bar{D}(x)^{\lambda D(x)}}{1+\bar{D}(x)^{\lambda D(x)}}$$

and

$$\gimel(x) = \frac{\lambda d(x)}{1+\bar{D}(x)^{\lambda D(x)}}\left(\{1+\log\bar{D}(x)\}D(x)-\log\bar{D}(x)\right) \tag{4}$$

2.1. Unique models of NHLG

We consider below some unique distributions for different supports of rvs $[(0,\,1),(0,\infty),(-\infty,\infty)]$, namely, for Beta (B), Kumaraswamy (Kw), Weibull (W), Fréchet (Fr) and Gumbel (Gu) models:

A. If $T \sim B(a,\,b)$ has the cdf $D(x) = I_x(a,\,b)$, $x \in (0,\,1)$ and pdf $d(x) = [B(a,\,b)]^{-1}\,x^{a-1}\,(1-x)^{b-1}$ then the cdf and pdf of the new half-logistic beta (NHLB) model are, respectively, given by

$$F_{\text{NHLB}}(x) = \frac{1-\left(1-I_x(a,\,b)\right)^{\lambda I_x(a,\,b)}}{1+\left(1-I_x(a,\,b)\right)^{\lambda I_x(a,\,b)}}, \quad x \in (0,\,1), \quad a,\,b>0$$

and

$$\begin{aligned} f_{\text{NHLB}}(x) =& 2\lambda x^{a-1}\,(1-x)^{b-1}\left(1-I_x(a,\,b)\right)^{\lambda I_x(a,\,b)} \\ &\times (1-I_x(a,\,b))^{-1}\left(1+\left\{1-I_x(a,\,b)\right\}^{\lambda I_x(a,\,b)}\right)^{-2} \\ &\times \left(I_x(a,\,b)+\left(I_x(a,\,b)-1\right)\log 1-I_x(a,\,b)\right) \end{aligned}$$

where

$$B(a,\,b)=\int\limits_0^1 z^{a-1}\,(1-z)^{b-1}\,dz,\quad B_z(a,\,b)=\int\limits_0^z z^{a-1}\,(1-z)^{b-1}\,dz$$

and

$$I_x(a,\,b)=\frac{B_z(a,\,b)}{B(a,\,b)}=\big(B(a,\,b)\big)^{-1}\int\limits_0^z z^{a-1}\,(1-z)^{b-1}\,dz$$

are the beta function, incomplete beta function, and incomplete beta function ratio, respectively.

B. If $T\sim \mathrm{Kw}(a,\,b)$ has the cdf $D(x)=1-(1-x^a)^b$ and pdf $d(x)=a\,b\,x^{a-1}\,(1-x^a)^{b-1}$, then the cdf and pdf of the NHLKw model are, respectively, given by

$$F_{\mathrm{NHLKw}}(x)=\frac{1-\big((1-x^a)^b\big)^{\lambda\left(1-(1-x^a)^b\right)}}{1+\big((1-x^a)^b\big)^{\lambda\left(1-(1-x^a)^b\right)}},\quad x\in(0,\,1),\quad a,\,b>0$$

and

$$f_{\mathrm{NHLKw}}(x)=2abx^{a-1}\,(x^a-1)^{-1}\left((1-x^a)^b\right)^{\lambda\left((1-x^a)^b+1\right)}\big(\big((1-x^a)^{-b}-1\big)-b\log(1-x^a)\big)$$

$$\times\big((1-x^a)^b\left(\log\left((1-x^a)^b\right)+1\right)-1\big)\left(\left((1-x^a)^b\right)^{\lambda}+\left((1-x^a)^b\right)^{\lambda(1-x^a)^b}\right)^{-2}$$

C. If $T\sim \mathrm{W}(\alpha,\,\beta)$ has the cdf $D(x)=1-\mathrm{e}^{-\alpha\,x^\beta}$, $x\in(0,\infty)$ and pdf $d(x)=\alpha\,\beta\,x^{\beta-1}\,\mathrm{e}^{-\alpha\,x^\beta}$, then the cdf and pdf of the new half-logistic Weibull (NHLW) model are, respectively, given by

$$F_{\mathrm{NHLW}}(x)=\frac{1-\left(\mathrm{e}^{-\alpha\,x^\beta}\right)^{\lambda[1-\mathrm{e}^{-\alpha\,x^\beta}]}}{1+\left(\mathrm{e}^{-\alpha\,x^\beta}\right)^{\lambda[1-\mathrm{e}^{-\alpha\,x^\beta}]}},\quad x\in(0,\infty),\quad \alpha,\,\beta>0$$

and

$$f_{\mathrm{NHLW}}(x)=2\alpha\beta\lambda x^{\beta-1}\left(\mathrm{e}^{\alpha\left(-x^\beta\right)}\right)^{\lambda+\lambda-\mathrm{e}^{\alpha\left(-x^\beta\right)}+1}\left(\mathrm{e}^{\alpha x^\beta}-\log\left(\mathrm{e}^{\alpha\left(-x^\beta\right)}\right)-1\right)$$

$$\times\left(\left(\mathrm{e}^{\alpha\left(-x^\beta\right)}\right)^{\lambda-\lambda\mathrm{e}^{\alpha\left(-x^\beta\right)}}+1\right)^{-2}$$

D. If $T\sim \mathrm{Fr}(a,\,b)$ has the cdf $D(x)=\mathrm{e}^{-a\,x^{-b}}$, $x\in(0,\infty)$ and pdf $d(x)=abx^{-b-1}\,\mathrm{e}^{-a\,x^{-b}}$, then the cdf and pdf of the new half-logistic Fréchet (NHLFr) model are, respectively, given by

$$F_{\mathrm{NHLFr}}(x)=\frac{1-\left(1-\mathrm{e}^{-a\,x^b}\right)^{\lambda(\mathrm{e}^{-a\,x^{-b}})}}{1+\left(1-\mathrm{e}^{-a\,x^{-b}}\right)^{\lambda(\mathrm{e}^{-a\,x^{-b}})}},\quad x\in(0,\infty),\quad a,\,b>0$$

and

$$f_{\text{NHLFr}}(x) = 2ab\lambda x^{-b-1}\mathrm{e}^{-ax^{-b}}\left(1-\mathrm{e}^{-ax^{-b}}\right)^{\lambda\mathrm{e}^{-ax^{-b}}-1}\left(\left(1-\mathrm{e}^{-ax^{-b}}\right)^{\lambda\mathrm{e}^{-ax^{-b}}}+1\right)^{-2}$$
$$\times\left(\mathrm{e}^{-ax^{-b}}\left(\log\left(1-\mathrm{e}^{-ax^{-b}}\right)+1\right)-\log\left(1-\mathrm{e}^{-ax^{-b}}\right)\right)$$

E. If $T\sim \text{Gu}(\mu,\sigma)$ has the cdf $D(x)=\mathrm{e}^{-\mathrm{e}^{(x-\mu)\,\sigma^{-1}}}$, $x\,\mu\in(-\infty,\infty)$ and pdf $d(x)=\sigma^{-1}\,\mathrm{e}^{(x-\mu)\,\sigma^{-1}}$ $\times\mathrm{e}^{-\mathrm{e}^{(x-\mu)\,\sigma^{-1}}}$, then the cdf and pdf of the new half-logistic Gumbel (NHLGu) model are, respectively, given by

$$F_{\text{NHLGu}}(x)=\frac{1-\left(1-\mathrm{e}^{-\mathrm{e}^{-(x-\mu/\sigma)}}\right)^{\mathrm{e}^{\left(-\mathrm{e}^{-(x-\mu/\sigma)}\right)}}}{1+\left(1-\mathrm{e}^{-\mathrm{e}^{-(x-\mu/\sigma)}}\right)^{\mathrm{e}^{\left(-\mathrm{e}^{-(x-\mu/\sigma)}\right)}}},\quad x\,,\mu\in(-\infty,\infty),\ \sigma>0$$

and

$$f_{\text{NHLGu}}(x)=\frac{2\lambda}{\sigma}\,\mathrm{e}^{-\frac{-\mu+\sigma\mathrm{e}^{\frac{\mu-x}{\sigma}}+x}{\sigma}}\left(1-\mathrm{e}^{-\mathrm{e}^{\frac{\mu-x}{\sigma}}}\right)^{\lambda\mathrm{e}^{-\mathrm{e}^{\frac{\mu-x}{\sigma}}}}\left(1-\mathrm{e}^{\mathrm{e}^{\frac{\mu-x}{\sigma}}}\right)$$
$$\left(\left(1-\mathrm{e}^{-\mathrm{e}^{\frac{\mu-x}{\sigma}}}\right)^{\lambda\mathrm{e}^{-\mathrm{e}^{\frac{\mu-x}{\sigma}}}}+1\right)^{-2}\left(\left(\mathrm{e}^{\mathrm{e}^{\frac{\mu-x}{\sigma}}}-1\right)\log\left(1-\mathrm{e}^{-\mathrm{e}^{\frac{\mu-x}{\sigma}}}\right)-1\right)$$

Figures 1–5 show some plots of density and hazard rate functions for various parameter combinations with different special models arising due to NHLG family. It is evident from these plots that the density of the NHLG family is adaptable to model varying real-life phenomenons. Further, the hazard rate function allows the risk evaluation of monotone and non-monotone failure rates.

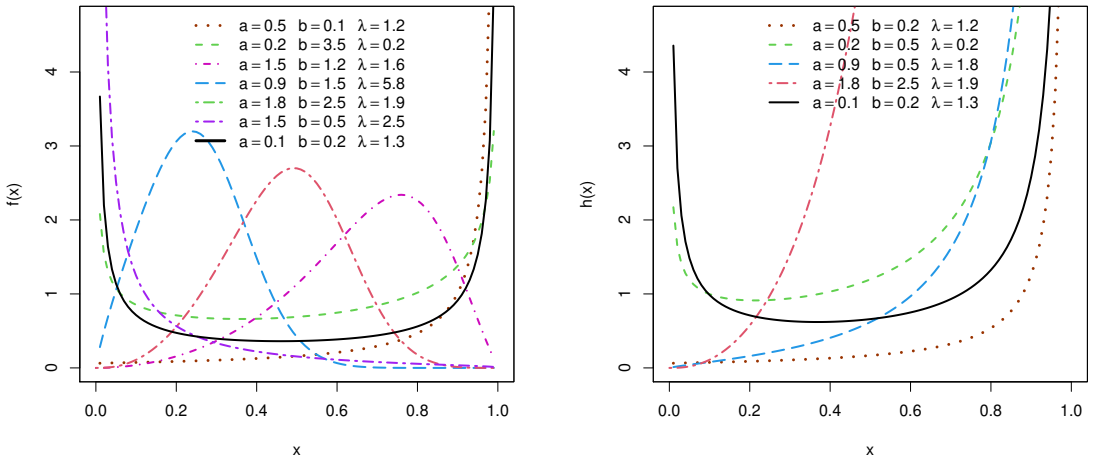

Figure 1. Plots for the NHLBeta model for some parameter values: density (right) and hazard rate (left)

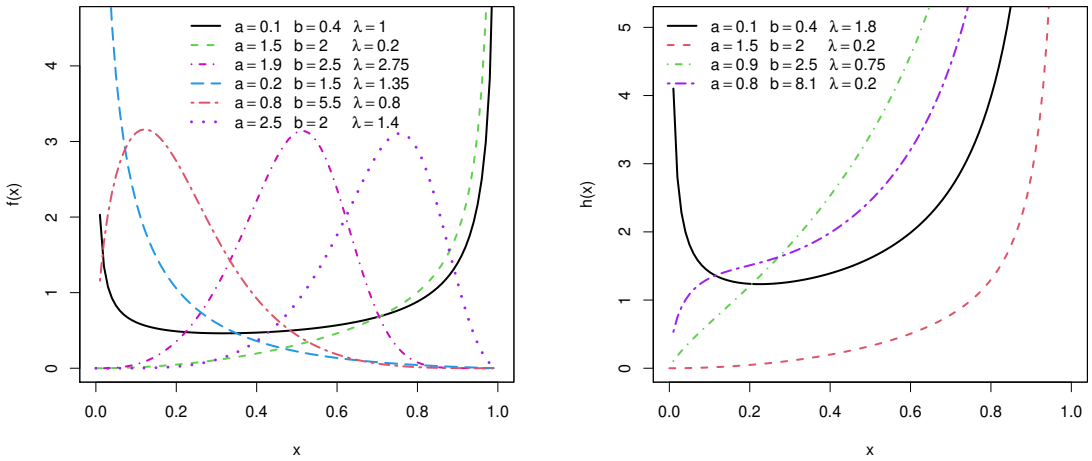

Figure 2. Plots for the NHLKw model for some parameter values: density (left) and hazard rate (right)

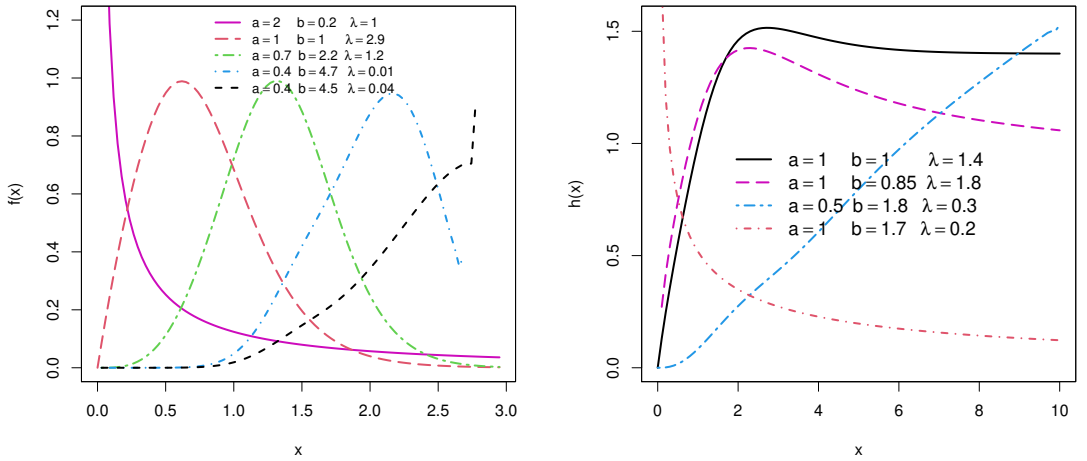

Figure 3. Plots for the NHLW model for some parameter values: density (left) and hazard rate (right)

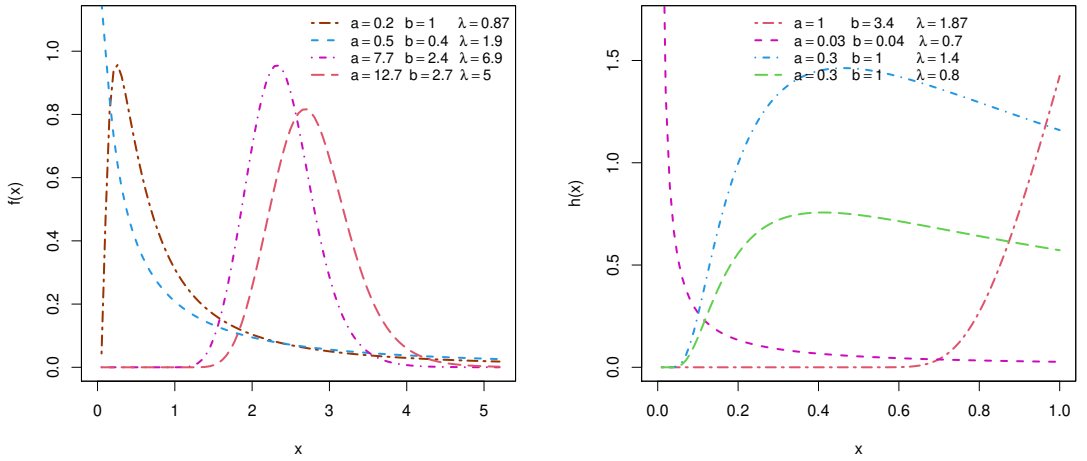

Figure 4. Plots for the NHLFr model for some parameter values: density (left) and hazard rate (right)

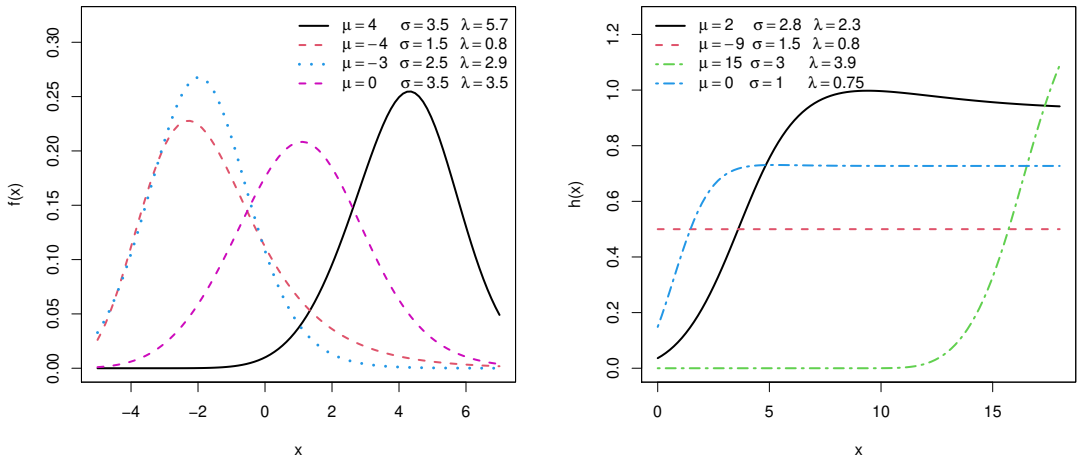

Figure 5. Plots for the NHLGu model for some parameter values: density (left) and hazard rate (right)

2.2. Useful expansion of NHLG

In this section, we demonstrate that the density function of X is expressible as an infinite linear combination of exponential-G (exp-G) densities. This is accomplished by first extending (2) in terms of cdf of exp-G densities and then differentiating it. Consider an arbitrary baseline cdf $D(x)$ with parameter $m > 0$, so that $Y \sim$ exp-G (m) with pdf and cdf in the formats as $H_m(x) = D(x)^m$ and $h_m(x) = md(x)D(x)^{m-1}$, respectively.

By using Mathematica on (2), the power series converges

$$F(x) = \sum_{\jmath=2}^{\infty} \omega_\jmath \, D(x)^\jmath \tag{5}$$

where $\omega_2 = \dfrac{\lambda}{2}$, $\omega_3 = \dfrac{\lambda}{4}$, $\omega_4 = \dfrac{\lambda}{6}$ and $\omega_5 = \dfrac{\lambda}{8}$, ..., which can be expressed as

$$F(x) = \sum_{\jmath=2}^{\infty} \omega_\jmath \, H_\jmath(x;\, \varsigma) \tag{6}$$

where $H_\jmath(x;\, \varsigma) = D(x;\, \varsigma)^\jmath$ (for $\jmath \geq 2$).

Differentiating (6), the resultant density of X takes the form

$$f(x) = \sum_{\jmath=1}^{\infty} \omega_{\jmath+1} \, h_{\jmath+1}(x;\, \varsigma) \tag{7}$$

where $h_{\jmath+1}$ is the exp-G density with power parameter $\jmath + 1$.

According to (7), the NHLG density function is a linear combination of exp-G densities. Hence, various mathematical properties of the NHLG can be determined directly from those of the exp-G distributions, which are known for several baseline distributions. For detailed discussion on exp-G distributions, we refer e.g. to Mudholkar and Srivastava [16], Gupta and Kundu [10], Nadarajah and Kotz [18].

2.3. Density and hazard rate shape

The shapes of the density and hrf can be described analytically. The critical points of the NHLG density are the roots of (3)

$$\lambda d(x)\log\bar{D}(x)+\frac{d'(x)}{d(x)}-\frac{d(x)\left(\lambda D(x)-1\right)}{\bar{D}(x)}+\frac{d(x)\left(2+\log\bar{D}(x)\right)}{-\log\bar{D}(x)+D(x)\left(1+\log\bar{D}(x)\right)} \tag{8}$$
$$-\frac{2\lambda d(x)\bar{D}(x)^{1+\lambda D(x)}}{1+\bar{D}(x)^{\lambda D(x)}}\Big(-1+\bar{D}(x)\left(1+\log\bar{D}(x)\right)\Big)=0$$

The critical points of the NHLG hrf are obtained from (4)

$$\frac{d'(x)}{d(x)}+\frac{d(x)}{\bar{D}(x)}+\frac{d(x)\left(2+\log\bar{D}(x)\right)}{-\log\bar{D}(x)+D(x)\{1+\log\bar{D}(x)\}} \tag{9}$$
$$-\frac{\lambda d(x)\bar{D}(x)^{1+\lambda D(x)}}{1+\bar{D}(x)^{\lambda D(x)}}\left(-1+\bar{D}(x)\left(1+\log\bar{D}(x)\right)\right)=0$$

2.4. Quantile function

The inverse cdf is the most straightforward way of creating rvs. In the case of any chosen cdf, the quantile function (qf) is defined as $Q(u)=F^{-1}(p)=\min\{x;\,F(x)\geq p\}$. Inverting the NHLG's qf in (2) and solving two non-linear equations numerically. We can use the following procedure:

(i) set $z=z(p)=1-p$

(ii) find $w=w(p)$ numerically in $w\log(1-w)=\log(z)$ using any Newton–Raphson algorithm;

(iii) numerical solution for x in $D(x;\,\xi)=w$ gives the qf $x=Q(p;\xi)$ of X.

2.5. Moments and generating function

The sth raw moment of X, say $\mathbb{E}(X^s)$, are expressed from (3) as

$$\mathbb{E}(X^s)=\sum_{\jmath=1}^{\infty}\omega_{\jmath+1}\,\mathbb{E}(Y_{\jmath+1}^s)=\sum_{\jmath=1}^{\infty}(\jmath+1)\,\omega_{\jmath+1}\,\tau_{s,\jmath} \tag{10}$$

where

$$\tau_{s,\jmath}=\int_{-\infty}^{\infty}x^s\,D(x;\,\varsigma)^{\jmath}\,d(x;\,\varsigma)dx=\int_0^1 Q_D(u;\varsigma)^s\,u^{\jmath}du,\,\text{and}Q_D(u;\varsigma)$$

is the qf of the baseline distribution.

Some characteristics of a distribution can be specified using the first four moments. Equation (10) can be helpful in determining the central moments and cumulants of X using well-established results.

The sth lower incomplete moment of X, say $m_s(y) = \int_{-\infty}^{y} x^s f(x)dx$, is

$$m_s(y) = \sum_{\jmath=1}^{\infty} \omega_{\jmath+1} \int_{-\infty}^{y} x^s h_{\jmath+1}(x)dx = \sum_{\jmath=1}^{\infty} (\jmath+1)\,\omega_{\jmath+1} \int_{0}^{D(y;\varsigma)} Q_D(u;\varsigma)^s u^{\jmath} du \tag{11}$$

For most G distributions, the final two integrals can be computed numerically.The total deviations from the mean and median are $\delta_1 = 2\mu_1' F(\mu_1') - 2m_1(\mu_1')$ and $\delta_2 = \mu_1' - 2m_1(M)$, where $F(\mu_1')$ comes from (2). The moment generating function (mgf) $M(t) = \mathbb{E}(\mathrm{e}^{tX})$ of X follows from (3) as

$$M(t) = \sum_{\jmath=1}^{\infty} \omega_{\jmath+1} M_{\jmath+1}(t) = \sum_{\jmath=0}^{\infty} (\jmath+1)\omega_{\jmath+1}\,\rho_{\jmath}(t), \tag{12}$$

where $M_{\jmath+1}(t)$ is the mgf of $Y_{\jmath+1}$ and $\rho_{\jmath}(t) = \int_{0}^{1} \exp(tQ_D(u;\varsigma))\,u^{\jmath}du$. Hence, $M(t)$ can be obtained from the exp-G generating function.

2.6. Estimation

We now look at how to use the maximum likelihood method to estimate the unknown parameters of a new distribution. Let $x_1, \ldots, x_n$ be n observations from the NHLG distribution given by (3) with parameter vector $\boldsymbol{\Xi} = (\lambda, \varsigma)^{\top}$. The log-likelihood $\ell = \ell(\boldsymbol{\Xi})$ for $\boldsymbol{\Xi}$ has the form

$$\begin{aligned} &n\log(2\lambda) + \sum_{i=1}^{n} (\lambda D(x_i;\varsigma) - 1)\log\left(1 - D(x_i;\varsigma)\right) - 2\sum_{i=1}^{n} \log\left(1 + \{1 - D(x_i;\varsigma)\}^{\lambda D(x_i;\varsigma)}\right) \\ &+ \sum_{i=1}^{n} \log d(x_i;\varsigma) + \sum_{i=1}^{n} \log\left(-\log\left(1 - D(x_i;\varsigma)\right) + D(x_i;\varsigma)\left(1 + \log\left(1 - D(x_i;\varsigma)\right)\right)\right) \end{aligned} \tag{13}$$

The MLE $\widehat{\boldsymbol{\Xi}}$ of $\boldsymbol{\Xi}$ can be evaluated by maximizing $\ell(\boldsymbol{\Xi})$. Several routines for numerical maximization of $\ell(\boldsymbol{\Xi})$ are easily available in the `SAS` (`PROC NLMIXED`), `R` program (`optim` function), `Ox` (sub-routine `MaxBFGS`), among others. We can also mitigate the nonlinear likelihood equations by differentiating the log-likelihood.

The consequent score components with respect to λ and ς are

$$\frac{\partial_l}{\partial_\lambda} = \frac{n}{\lambda} + \sum_{i=1}^{n} \log D(x_i;\varsigma)[1 - D(x_i;\varsigma)]$$

$$- 2\sum_{i=1}^{n} \frac{-\log[1 - D(x_i;\varsigma)]D(x_i;\varsigma)[1 - D(x_i;\varsigma)]^{\lambda D(x_i;\varsigma)}}{1 + [1 - D(x_i;\varsigma)]^{-\lambda D(x_i;\varsigma)}}$$

$$\frac{\partial_l}{\partial_\varsigma} = \sum_{i=1}^{n} d(x_i;\varsigma) d_i^{\varsigma} \left(\lambda \, \log(1 - D(x_i)) - \frac{\lambda D(x_i) - 1}{1 - D(x_i)} \right) + \sum_{i=1}^{n} \frac{d_i^{\varsigma}}{d(x_i;\varsigma)}$$

$$+ \sum_{i=1}^{n} \frac{d_i^{\varsigma} d(x_i;\varsigma) \left(1 + \{\log[1 - D(x_i)] - D(x_i)\}\right)}{[1 - D(x_i)]\big(- \log[1 - D(x_i)] + D(x_i)\{1 + \log[1 - D(x_i)]\}\big)}$$

$$- 2 \sum_{i=1}^{n} \frac{\lambda d_i^{\varsigma} d(x_i;\varsigma)(1 - D(x_i))^{\lambda D(x_i)} \left(\log(1 - D(x_i)) + D(x_i)(1 - D(x_i))^{-1}\right)}{[1 - D(x_i)][1 + (1 - D(x_i))^{\lambda D(x_i)}]}$$

The MLEs of the model parameters are achieved by determining the score components to zero and solving them all at the same time. The resulting equations cannot be solved analytically, but they can be solved numerically using iterative Newton–Raphson type procedures in some statistical software.

For interval estimation and hypothesis tests on the model parameters, we can obtain the $(v+1)\times(v+1)$ observed information matrix $J(\Xi)$ numerically (v is the dimension of ς) since the expected information matrix $K(\Xi)$ is very complex and requires numerical integration.

Under standard regularity conditions, we have $(\widehat{\Xi}\Xi) \overset{a}{\sim} \mathcal{N}_{v+2}(0, K(\Xi)^{-1})$, where $\overset{a}{\sim}$ means approximately distributed and $K(\Xi)$ is the expected information matrix. The asymptotic behavior remains valid if $K(\Xi)$ is replaced by the observed information matrix $J(\Xi)$ evaluated at $\widehat{\Xi}$, that is, $J(\widehat{\Xi})$. Approximate confidence intervals for model parameters can be constructed using the multivariate normal $\mathcal{N}_{v+2}(0, J(\widehat{\Xi})^{-1})$ distribution.

3. New half logistic Fréchet (NHLFr) distribution

3.1. The model

We define the NHLFr distribution of Section 2 (case (iv)) with cdf and pdf

$$F_{NHLFr}(x;\ a,\ b) = \frac{1 - \left(1 - \mathrm{e}^{-a\,x^{b}}\right)^{\lambda(\mathrm{e}^{-a\,x^{-b}})}}{1 + \left(1 - \mathrm{e}^{-a\,x^{-b}}\right)^{\lambda(\mathrm{e}^{-a\,x^{-b}})}}, \quad x \in (0,\infty), \quad a,\, b > 0 \tag{14}$$

and

$$\begin{aligned} f_{NHLFr}(x;\ a,b) =& 2\,ab\lambda x^{-b-1}\mathrm{e}^{-ax^{-b}} \left(1 - \mathrm{e}^{-ax^{-b}}\right)^{\lambda(\mathrm{e}^{-ax^{-b}})-1} \left(\left(1 - \mathrm{e}^{-ax^{-b}}\right)^{\lambda\mathrm{e}^{-ax^{-b}}} + 1\right)^{-2} \\ & \times \left(\mathrm{e}^{-ax^{-b}} \left(\log\left(1 - \mathrm{e}^{-ax^{-b}}\right) + 1\right) - \log\left(1 - \mathrm{e}^{-ax^{-b}}\right)\right) \end{aligned} \tag{15}$$

Let X be an rv having density given by (15). The sf and hrf of X have, respectively, the forms

$$S_{\text{NHLFr}}(x;\ a,\ b) = 1 - \frac{1 - \left(1 - \mathrm{e}^{-a\,x^{b}}\right)^{\lambda(\mathrm{e}^{-a\,x^{-b}})}}{1 + \left(1 - \mathrm{e}^{-a\,x^{-b}}\right)^{\lambda(\mathrm{e}^{-a\,x^{-b}})}}$$

and

$$\pi_{\text{NHLFr}}(x;\ a,\ b) = \frac{ab\lambda x^{-b-1}\mathrm{e}^{-ax^{-b}}\left(\left(\mathrm{e}^{ax^{-b}} - 1\right)\log\left(1 - \mathrm{e}^{-ax^{-b}}\right) - 1\right)}{1 - \left(\mathrm{e}^{ax^{-b}}\right)\left(\left(1 - \mathrm{e}^{-ax^{-b}}\right)^{\lambda\mathrm{e}^{-ax^{-b}}} + 1\right)}$$

3.2. Quantile

The qf of NHLFr distribution cannot be accessed directly. However, we can create NHLFr variates using the Newton–Raphosn algorithm as follows:

1. Set the default values for n, a, b, λ and x_0.
2. Create U$\sim$Uniform$(0,\ 1)$.
3. Employing Newton–Raphson's algorithm given below, modify $x0$ each time as

   $$x_* = x_0 - R(x_0; a,\ b, \lambda),$$

   where $R(x_0; a,\ b, \lambda) = \dfrac{F_{NHLFr}(x_0; a,\ b, \lambda)}{f_{NHLFr}(x_0; a,\ b, \lambda)}$, and F_{NHLFr} and f_{NHLFr} are obtained from (14) and (15), respectively.
4. If $|x_0 - x_*| \leq \epsilon$, ($\epsilon > 0$, very small tolerance limit), then store $x_0 = x_*$ as a variate from the NHLFr(a, b, λ) distribution.
5. If $|x_0 - x_*| > \epsilon$, then, set $x_0 = x_*$ and move to step 3.
6. To generate $x_1, \ldots, x_n$, steps (2)–(5) are repeated n times.

3.3. Mathematical properties

Following the result from (6), the linear representation of NHLFr is quite straightforward as

$$F_{NHLFr}(x;\ a,\ b,\ \lambda) = \sum_{\jmath=2}^{\infty} \omega_{\jmath}\ \left(\mathrm{e}^{a\,x^{-b}}\right)^{\jmath}, \quad \jmath \geq 2 \tag{16}$$

By differentiating the last expression, we obtain the density of NHLFr as

$$f_{NHLFr}(x;\ a,\ b,\ \lambda) = \sum_{\jmath=1}^{\infty} \omega_{\jmath}\, \Pi(x;\ a\jmath,\ b) \tag{17}$$

where $\Pi(x;\ a\jmath,\ b)$ denotes the Fréchet density with shape parameter b.

Let W be an rv with density $\Pi(x;\ a\jmath,\ b)$, then we can extract several properties of X from those of W. First, the sth ordinary moment of X takes the form

$$\mu'_s = \sum_{k=1}^{\infty} \omega_\jmath \frac{(a\,\jmath)^{2-s/b}}{\Gamma\left(1-\frac{s}{b}\right)} \tag{18}$$

The cumulants (κ_n) of X can be determined recursively from (18) as $\kappa_s = \mu'_s - \sum_{k=1}^{s-1} \binom{s-1}{k-1} \kappa_k\, \mu'_{s-k}$, respectively, where $\kappa_1 = \mu'_1$. Table 1 provides some numerical results for the central moments for NHLFr distribution.

Table 1. Some moments of NHLFr $(a,\ b,\ \lambda)$ distribution for chosen parameters

a	b	λ	μ'_1	μ'_2	μ'_3	μ'_4	σ^2	σ
0.2	0.5	1.5	0.964	3.648	21.432	150.901	2.719	1.649
0.2	1.5	1.5	0.724	2.837	17.002	120.839	2.312	1.521
0.2	2.3	1.5	0.832	0.882	1.711	33.652	0.190	0.436
0.2	3.8	1.5	0.875	0.822	0.850	1.031	0.057	0.238
0.1	1.5	1.35	0.588	1.302	79.651	1916.734	0.956	0.978
0.1	1.5	2.2	0.373	0.192	0.213	4.656	0.053	0.229
0.1	1.5	3.5	0.292	0.101	0.042	0.024	0.015	0.123
0.1	1.5	5.5	0.242	0.065	0.019	0.006	0.006	0.079

Second, the sth incomplete moments of X is $\zeta_s(y) = \int_0^y x^s f_{NHLFr}(x;\ a,\ b)dx$, which can easily be calculated by applying standard transformations such as $u^{-v}\Gamma(v, ux) = \int_0^z z^{v-1}\mathrm{e}^{-ux}dz$ for each respective moment of W. The result thus obtained is as follows

$$\zeta_s = \sum_{k=1}^{\infty} \omega_\jmath \left(\frac{(a\,\jmath)^{2-(s/b)}}{\Gamma\left(1-\frac{s}{b}\right)} - \frac{\Gamma\left(1-\frac{s}{b}, a\,W\right)}{a^{1-\frac{s}{b}}} \right) \tag{19}$$

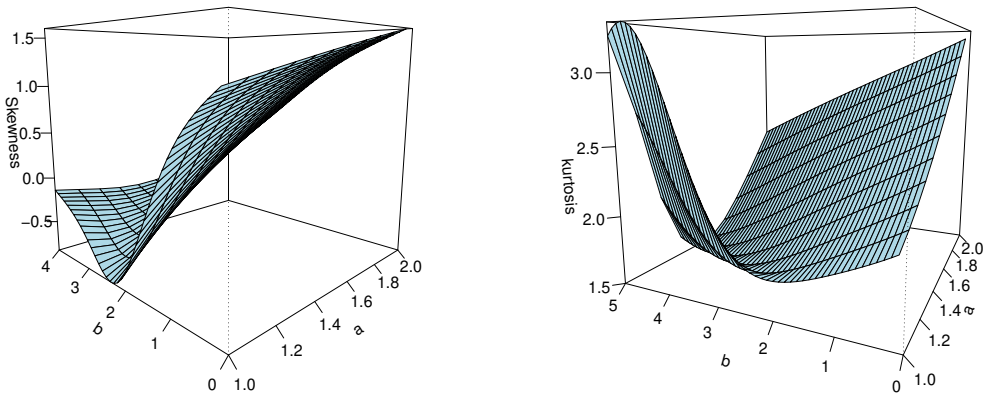

Figure 6. Plots of skewness and kurtosis for the NHLFr model

The total deviations from the mean μ_1' and median M of X have the forms $\delta_1 = 2\mu_1' F_{NHLFr}(\mu_1') - 2m_1(\mu_1')$ and $\delta_2 = \mu_1' - 2m_1(M)$, where M can be determined from $F_{NHLFr}(M) = 0.5$ The first incomplete moment $m_1(y)$ is also used to construct the Bonferroni and Lorenz curves (popular inequality measures in economics, reliability, demography and actuarial sciences). The Bonferroni and Lorenz curves of X for a given probability π are given by $B(\pi) = m_1(q)/(\pi\, mu_1')$ and $L(\pi) = \pi\, B(\pi)$, respectively, where $q = Q_\pi$ is the qf of X discussed in Section 2.5. The skewness and kurtosis plots of the NHLFr distribution are graphed in Figure 6. These plots reveal that the parameters a and b play a significant role in enhancing the skewness and kurtosis behaviors of X.

3.4. Estimation

The log-likelihood $\ell = \ell(\boldsymbol{\Xi})$ for $\boldsymbol{\Xi}$ has the form

$$\begin{aligned}\ell(\boldsymbol{\Xi}) =& n\log(2\,\lambda) + \sum_{i=1}^{n}\left(\lambda \mathrm{e}^{-a x_i^{-b}} - 1\right)\log\left(1-\mathrm{e}^{-a x_i^{-b}}\right)\\ &- 2\sum_{i=1}^{n}\log\left(\left(1-\mathrm{e}^{-a x_i^{-b}}\right)^{\lambda \mathrm{e}^{-a x_i^{-b}}} + 1\right) + \sum_{i=1}^{n}\log\left(abx_i^{-b-1}\mathrm{e}^{-a\, x_i^{-b}}\right)\\ &+ \sum_{i=1}^{n}\log\left(\mathrm{e}^{-a x_i^{-b}}\left\{1+\log\left(1-\mathrm{e}^{-a x_i^{-b}}\right)\right\} - \log\left(1-\mathrm{e}^{-a x_i^{-b}}\right)\right)\end{aligned} \tag{20}$$

The components of score vector $U(\Xi)$ are

$$\frac{\partial_l}{\partial_\lambda} = \frac{n}{\lambda} + \mathrm{e}^{-a x_i^{-b}}\log\left(1-\mathrm{e}^{-a x_i^{-b}}\right) - \frac{2\,\mathrm{e}^{-a x_i^{-b}}\left(1-\mathrm{e}^{-a x_i^{-b}}\right)^{\lambda \mathrm{e}^{-a x_i^{-b}}}\log\left(1-\mathrm{e}^{-a x_i^{-b}}\right)}{\left(1-\mathrm{e}^{-a x_i^{-b}}\right)^{\lambda \mathrm{e}^{-a x_i^{-b}}} + 1}$$

$$\begin{aligned}\frac{\partial_l}{\partial_a} =& \frac{n}{a} - \sum_{i=1}^{n} x_i^{-b}\left(1+\lambda \mathrm{e}^{-a x_i^{-b}}\right) + \sum_{i=1}^{n}\frac{x_i^{-b}\left(1-\lambda \mathrm{e}^{-a x_i^{-b}}\right)}{1-\mathrm{e}^{a x_i^{-b}}}\\ &+ \sum_{i=1}^{n}\frac{x_i^{-b}\left(\log\left(1-\mathrm{e}^{-a x_i^{-b}}\right)+2\right)}{\left(\mathrm{e}^{a x_i^{-b}}-1\right)\log\left(1-e^{-a x_i^{-b}}\right)-1}\\ &+ \frac{2\lambda x_i^{-b}\mathrm{e}^{-a x_i^{-b}}\left(1-\mathrm{e}^{-a x_i^{-b}}\right)^{\lambda \mathrm{e}^{-a x_i^{-b}}}\left(\left(\mathrm{e}^{a x_i^{-b}}-1\right)\log\left(1-\mathrm{e}^{-a x_i^{-b}}\right)-1\right)}{\left(\mathrm{e}^{a x_i^{-b}}-1\right)\left(\left(1-\mathrm{e}^{-a x_i^{-b}}\right)^{\lambda \mathrm{e}^{-a x_i^{-b}}}+1\right)}\end{aligned}$$

$$\frac{\partial_l}{\partial_b} = \frac{n}{b} - \sum_{i=1}^{n} \log(x_i)\left(1 + a\, x_i^{-b}\right) + a\lambda \sum_{i=1}^{n} x_i^{-b} \log(x_i)\, \mathrm{e}^{-a x_i^{-b}} \log\left(1 - \mathrm{e}^{-a x_i^{-b}}\right)$$

$$+ a \sum_{i=1}^{n} \frac{x_i^{-b} \log(x_i)\, \mathrm{e}^{-a x_i^{-b}} \left(\mathrm{e}^{a x_i^{-b}} - \lambda\right)}{\mathrm{e}^{a x_i^{-b}} - 1} + a \sum_{i=1}^{n} \frac{x_i^{-b} \log(x_i) \left(2 + \log\left(1 - \mathrm{e}^{-a x_i^{-b}}\right)\right)}{\left(\mathrm{e}^{a x_i^{-b}} - 1\right) \log\left(1 - \mathrm{e}^{-a x_i^{-b}}\right) - 1}$$

$$- 2\, a\lambda \sum_{i=1}^{n} \frac{x_i^{-b} \log(x_i)\, \mathrm{e}^{-a x_i^{-b}} \left(1 - \mathrm{e}^{-a x_i^{-b}}\right)^{\lambda \mathrm{e}^{-a x_i^{-b}}} \left(\left(\mathrm{e}^{a x_i^{-b}} - 1\right) \log\left(1 - \mathrm{e}^{-a x_i^{-b}}\right) - 1\right)}{\left(\mathrm{e}^{a x_i^{-b}} - 1\right) \left(\left(1 - \mathrm{e}^{-a x_i^{-b}}\right)^{\lambda \mathrm{e}^{-a x_i^{-b}}} + 1\right)}$$

The observed information matrix for the parameter vector $\Xi = (a,\ b, \lambda)^{\top}$ is given by

$$J(\Xi) = -\frac{\partial^2 \ell(\Xi)}{\partial \Xi\, \partial \Xi^{\top}} = -\begin{pmatrix} J_{aa} & J_{ab} & J_{a\lambda} \\ \cdot & J_{bb} & J_{b\lambda} \\ \cdot & \cdot & J_{\lambda\lambda} \end{pmatrix}$$

3.5. Simulation

In this subsection, a simulation study with varying sample sizes is performed. The aim is to assess the performance of NHLFr model parameter vector ($\Xi = \alpha, \beta, \lambda$) with their respective estimates ($\hat{\Xi} = \hat{\alpha}, \hat{\beta}, \hat{\lambda}$). The parameters are estimated by maximizing the log-likelihood function in (20), following the method of maximum likelihood estimation (MLEs) using the optim routine in R software. The defining criterion includes the computation of average bias (Bias), mean squared errors (MSEs), coverage probability (CP), average lower bounds (ALB)and average upper bounds (AUB) for the two-sided confidence intervals of the model parameters. We considered the surety levels to be 90% and 95% by adopting the following steps.

A. We generate 1000 random samples $x_1, x_2, \ldots, x_n$ of given sizes n from the NHLFr distribution.

B. The considered sets of parameter values are: set I ($\alpha = 3.5$, $\beta = 3.8$ and $\lambda = 4.9$), set II ($\alpha = 2.35$, $\beta = 3.85$ and $\lambda = 2.9$) and set III ($\alpha = 2.5$, $\beta = 4.1$ and $\lambda = 3.85$).

C. The numerical results are calculated at the surety mentioned above levels.

The obtained results are given in Tables 2–4. The simulation findings clearly verify, in general, that the biases and MSEs decrease as a result of an increase in sample size to true parameter values. The CP of the confidence interval is quite close to the respective surety levels (90% and 95%) nominal level. The average length of the confidence interval of each respective parameter also stabilizes with the increase in sample size which confirms that these asymptotic results are useful in the estimation and construction of confidence intervals. Further, plots of Biases and MSEs for the parameters a, b and λ at selective sample sizes are displayed in Figures 7–9. The plots further ascertain that a drastic decrease in biases and MSEs occurs with a certain increase in the sample size n. Thus, the MLEs perform well in estimating the parameters of the NHLFr distribution.

Table 2. Simulation results for set I

Ξ	n	$\hat{\Xi}$	Bias	MSEs	$CP_{90\%}$	$ALB_{90\%}$	$AUB_{90\%}$	$CP_{95\%}$	$ALB_{95\%}$	$AUB_{95\%}$
a	50	4.455	0.955	8.672	0.96	3.803	5.106	0.99	3.742	5.802
	100	3.906	0.406	0.604	0.97	3.797	4.016	0.98	3.721	3.952
	150	3.674	0.174	0.223	0.96	3.615	3.733	0.99	3.642	3.754
	200	3.609	0.169	0.177	0.97	3.579	3.639	0.99	3.606	3.692
	250	3.643	0.143	0.113	0.91	3.611	3.675	0.98	3.599	3.688
	300	3.623	0.123	0.093	0.95	3.597	3.650	0.98	3.524	3.553
	500	3.539	0.039	0.029	0.94	3.527	3.551	0.98	3.500	3.563
	600	3.546	0.026	0.025	0.92	3.535	3.556	0.97	3.525	3.561
b	50	4.209	0.409	4.190	0.98	3.740	4.678	0.99	3.712	5.137
	100	4.148	0.348	2.027	0.94	3.919	4.376	0.99	3.704	4.209
	150	3.893	0.093	1.265	0.95	3.742	4.045	1.00	6.296	9.142
	200	3.856	0.056	0.489	0.99	3.778	3.934	0.98	3.796	4.026
	250	3.855	0.055	0.449	0.97	3.782	3.927	0.97	3.743	4.001
	300	3.935	0.035	0.514	0.94	3.868	4.002	0.97	3.814	3.968
	500	3.830	0.030	0.242	0.97	3.797	3.863	0.98	3.800	3.886
	600	3.806	0.016	0.201	0.95	3.827	3.905	0.97	3.827	3.901
λ	50	37.561	32.661	22140.547	1.00	3.619	71.503	1.0	7.270	132.375
	100	16.065	11.165	3217.455	0.99	6.871	25.260	1.0	6.741	11.956
	150	11.755	6.855	1159.519	0.97	7.252	16.257	0.99	6.296	9.142
	200	5.886	1.094	19.427	0.98	5.542	6.436	0.99	5.543	6.766
	250	5.994	0.986	15.062	0.95	5.442	6.336	0.97	5.539	6.228
	300	5.465	0.565	8.319	0.99	5.195	5.735	0.98	5.272	5.823
	500	5.252	0.352	3.108	0.96	5.124	5.379	0.98	5.102	5.510
	600	5.074	0.228	1.446	0.91	5.004	5.253	0.98	4.939	5.210

Table 3. Simulation results for set II

Ξ	n	$\hat{\Xi}$	Bias	MSEs	$CP_{90\%}$	$ALB_{90\%}$	$AUB_{90\%}$	$CP_{95\%}$	$ALB_{95\%}$	$AUB_{95\%}$
a	50	2.716	0.366	0.463	0.94	2.582	2.850	0.98	2.573	2.906
	100	2.537	0.187	0.158	0.93	2.479	2.595	0.98	2.481	2.617
	150	2.427	0.177	0.062	0.90	2.395	2.459	0.96	2.406	2.501
	200	2.360	0.110	0.031	0.96	2.339	2.380	0.96	2.376	2.431
	250	2.394	0.044	0.033	0.88	2.376	2.413	0.95	2.361	2.406
	300	2.371	0.021	0.026	0.91	2.356	2.386	0.96	2.372	2.406
	500	2.372	0.022	0.022	0.87	2.362	2.383	0.95	2.355	2.378
	600	2.351	0.019	0.012	0.87	2.345	2.376	0.95	2.342	2.269
b	50	4.184	0.334	3.655	1.00	3.744	4.625	1.00	3.576	4.474
	100	3.886	0.336	1.267	0.85	3.700	4.072	0.95	3.628	4.193
	150	3.999	0.149	0.718	0.88	3.887	4.112	0.86	3.781	4.077
	200	3.965	0.115	0.570	0.92	3.878	4.053	0.78	3.871	4.090
	250	3.844	0.106	0.338	0.95	3.783	3.905	0.89	3.784	3.936
	300	3.783	0.067	0.271	0.93	3.734	3.832	0.98	3.830	3.961
	500	3.855	0.045	0.256	0.89	3.768	3.843	0.91	3.921	4.095
	600	3.851	0.005	0.196	0.90	3.728	3.839	0.90	3.828	4.085
λ	50	10.542	7.652	1164.711	0.98	2.766	18.318	1.00	1.998	21.219
	100	4.649	1.759	22.189	1.00	3.926	5.371	0.99	3.784	7.628
	150	3.392	0.502	5.854	0.99	3.072	3.711	1.00	3.138	3.850
	200	3.171	0.281	2.379	1.00	2.993	3.348	1.00	2.977	3.453
	250	3.174	0.284	1.140	0.99	3.066	3.282	1.00	3.040	3.309
	300	3.239	0.249	1.107	0.98	3.144	3.333	1.00	3.006	3.244
	500	3.153	0.263	0.846	0.95	3.088	3.218	0.99	2.801	2.997
	600	3.003	0.164	0.349	0.95	2.988	3.027	0.98	2.821	2.951

Table 4. Simulation results for set III

Ξ	n	$\hat{\Xi}$	Bias	MSEs	$CP_{90\%}$	$ALB_{90\%}$	$AUB_{90\%}$	$CP_{95\%}$	$ALB_{95\%}$	$AUB_{95\%}$
a	50	5.030	2.180	249.886	0.96	1.370	8.691	0.98	2.063	6.915
	100	3.121	0.271	0.295	0.96	3.043	3.199	0.96	3.011	3.232
	150	2.984	0.134	0.133	0.92	2.938	3.030	0.96	2.946	3.043
	200	2.947	0.097	0.091	0.89	2.914	2.981	0.96	2.971	3.035
	250	2.906	0.056	0.041	0.94	2.885	2.926	0.96	2.916	2.973
	300	2.897	0.047	0.042	0.88	2.878	2.916	0.97	2.893	2.939
	500	2.781	0.025	0.029	0.90	2.867	2.895	0.95	2.887	2.919
	600	2.657	0.022	0.026	0.90	2.842	2.895	0.95	2.880	2.909
b	50	5.022	0.972	14.163	0.95	4.172	5.872	0.99	3.466	5.270
	100	4.089	0.039	1.571	0.97	3.882	4.297	0.98	3.849	4.427
	150	4.193	0.143	1.042	0.86	4.056	4.329	0.99	3.967	4.253
	200	4.139	0.089	0.772	0.85	4.037	4.241	0.96	3.972	4.220
	250	4.127	0.077	0.552	0.77	4.049	4.204	0.87	4.106	4.284
	300	4.063	0.013	0.445	0.98	3.999	4.126	0.84	4.006	4.166
	500	3.990	0.009	0.261	0.92	3.889	3.971	0.81	3.963	4.095
	600	3.977	0.007	0.204	0.92	3.819	3.979	0.91	3.959	4.821
λ	50	8.936	5.086	613.884	1.00	3.266	14.605	0.99	7.847	125.833
	100	13.801	9.951	4188.593	0.99	3.228	24.373	0.99	5.825	11.575
	150	5.053	1.203	27.910	0.99	4.359	5.748	0.98	4.430	5.552
	200	4.800	0.950	18.149	1.00	4.315	5.286	0.99	4.599	5.465
	250	4.446	0.596	7.480	0.97	4.167	4.725	1.00	3.975	4.488
	300	4.329	0.479	2.840	0.97	4.175	4.483	0.98	3.988	4.665
	500	4.151	0.411	2.271	0.99	4.037	4.565	0.96	3.376	4.824
	600	3.952	0.237	1.950	0.99	3.577	4.005	0.95	3.369	4.117

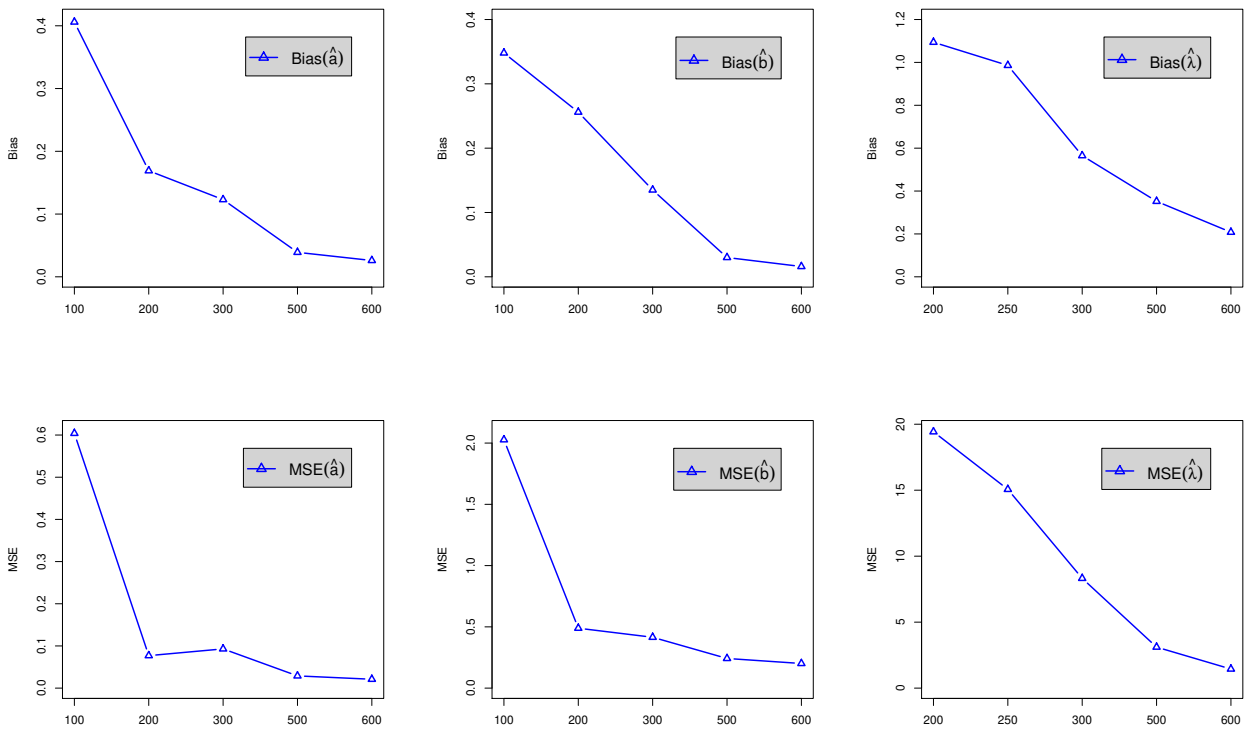

Figure 7. Plots of the Biases and MSEs for specific parameter values for set I

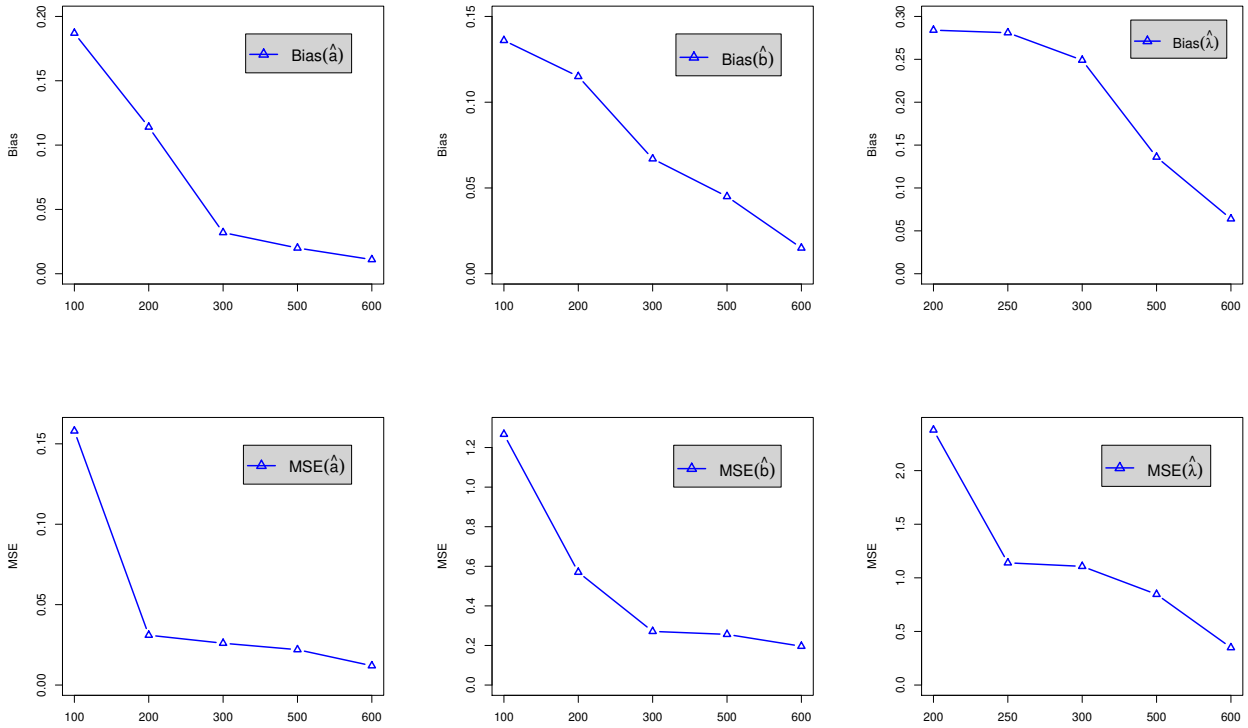

Figure 8. Plots of the Biases and MSEs for specific parameter values for set II

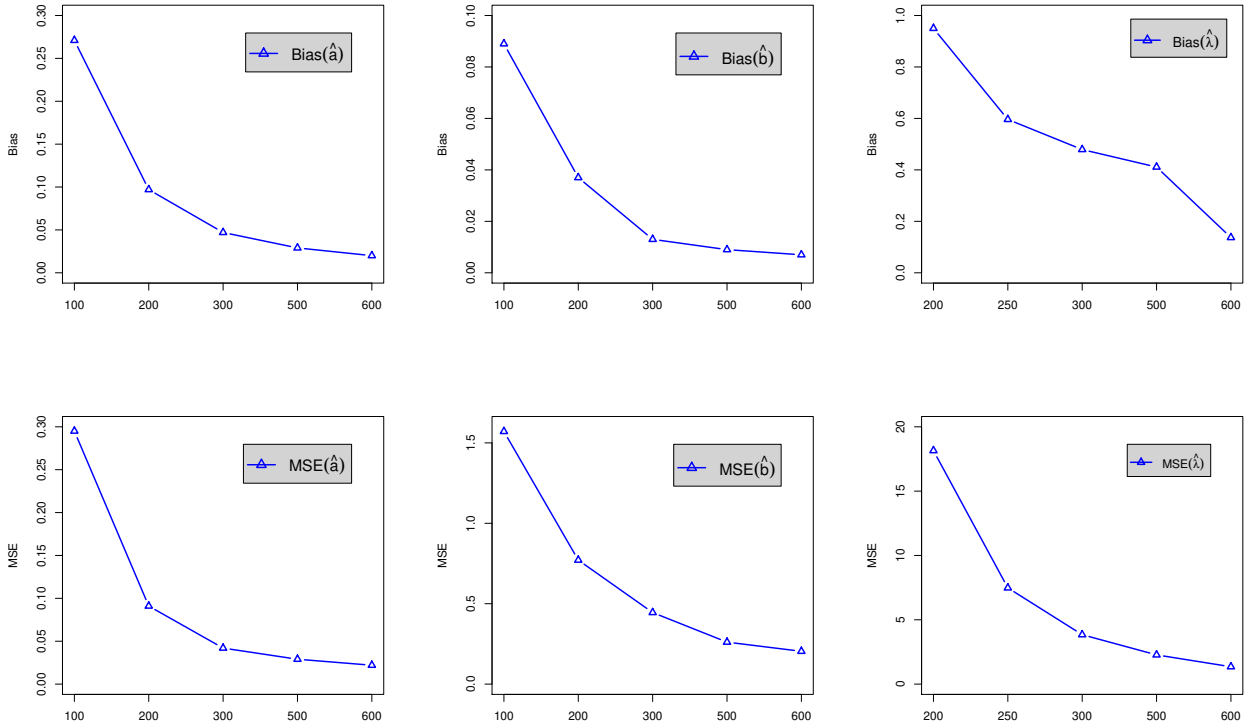

Figure 9. Plots of the Biases and MSEs for specific parameter values for set III

3.6. Analysis of COVID-19 and cancer data

Even if numerous bounded distributions exist in the literature, no single distribution can be deemed the best for describing all types of data. In this section, we apply the NHLFr lifetime model for the statistical analysis of three real-life healthcare data sets. The first data set, denoted by cancer data, represents the remission times (in months) of a random sample of 128 bladder cancer patients. The second data set, denoted by Covid 1, signifies the daily confirmed cases of COVID-19 (per day) in Pakistan. The third data reported by the World Health Organization (WHO), denoted by Covid 2, manifests the number of deaths reported in the last 24 hours globally. In particular, we aim to compare the fits of the NHLFr model with other generalizations of the Fréchet (Fr) models given in Table 5. The parameters are all positive real numbers of these densities.

Table 5. The comparative fitted models

Distribution	Authors
BFr	Nadarajah and Gupta [17], Barreto and Souza ([4])
EGFr	Cordiero et al. [6]
HLFr	Cordiero et al. [5]
EFr	Nadarajah and Kotz [11]
ZBGaFr	Da Silva et al. [7]
TLIW	Salman Abbas et al. [1]
MOFr	Krishna et al. [12]
Fr	Fréchet [8]

We use the method of maximum likelihood estimation to estimate the unknown parameters as presented in Section 3.4. For each dataset, we consider the following criteria when making a suitable comparison: the minus log-likelihood ($\hat{-\ell}$) of the model taken at the corresponding MLEs, the Akaike information criterion (AICs), Bayesian information criterion (BICs), Anderson–Darling (AD), Cramér–von Mises (CvM) and Kolmogrov–Smirnov (KS) as well as the p-value (PV) of the related KS test. They are, respectively, defined by

$$\mathrm{AIC} = -2\hat{\ell} + 2p, \quad \mathrm{BIC} = -2\hat{\ell} + p\log(n)$$

$$\mathrm{AD} = -\left(\frac{2.25}{n^2} + \frac{0.75}{n} + 1\right)\left(n + \frac{1}{n}\sum_{i=1}^{n}(2i-1)\left(\log y_i + \log(1-y_{n-i+1})\right)\right)$$

$$\mathrm{CvM} = \left(\frac{0.5}{n} + 1\right)\left(\sum_{i=1}^{n}\left(y_i - \frac{2i-1}{2n}\right) + \frac{1}{12n}\right), \quad \mathrm{KS} = \max\left(\frac{i}{n} - y_i,\, y_i - \frac{i-1}{n}\right)$$

and PV$= (D_n \geq KS)$ with $D_n = \sup_{x\in\mathbb{R}}|F_n(x) - \hat{F}(x)|$, where p is the number of parameters of the considered model, $x_{(1)}, \ldots, x_{(n)}$ are the ordered observations and $y_i = \hat{F}(x_{(i)})$ is the empirical cdf defined from 14. The required computations are carried out using the R script `AdequacyModel` which is easily available from http://cran.rproject.org/web/packages/AdequacyModel/AdequacyModel.pdf. For each criterion (except PV(K-S) with the highest value), the smallest values is gained by the NHLFr model, indicating that it provides the best fit. Finally, the asymptotic confidence intervals (CIs) of the NHLFr parameters at different surety levels (95% and 99%) alongside the variance-covariance matrix, respectively, are also provided.

3.6.1. Cancer data

The data set comprises the remission times (in months) of a random sample of 128 bladder cancer patients originally studied by [13]. Some descriptive statistics related to this data are given in Table 6. The skewness and kurtosis are indicative of exponentially tailed data (reversed-J shape). The TTT plot alongside the fitted hazard rate function is given in Figure 10. In particular, the TTT plot shows a possible increasing-decreasing hrf permitting fitting NHLFr model on this data set. The MLEs (with SEs in parenthesis), AICs, BICs, AD, CvM and PV(K-S), are listed in Table 7. For a more visual view, the estimated pdf, cdf, PP and Q-Q plots are displayed in Figure 11 of the NHLFr model. The figure shows nice fits for the NHLFr model. Finally, the asymptotic confidence intervals of the NHLFr parameters are presented in Table 8 with the levels 95% and 99%.

Table 6. The descriptive statistics of cancer data set

Sample size	Mean	Median	SD	Minimum	Maximum	Skewness	Kurtosis
128	9.37	6.40	10.51	0.08	79.05	3.29	15.48

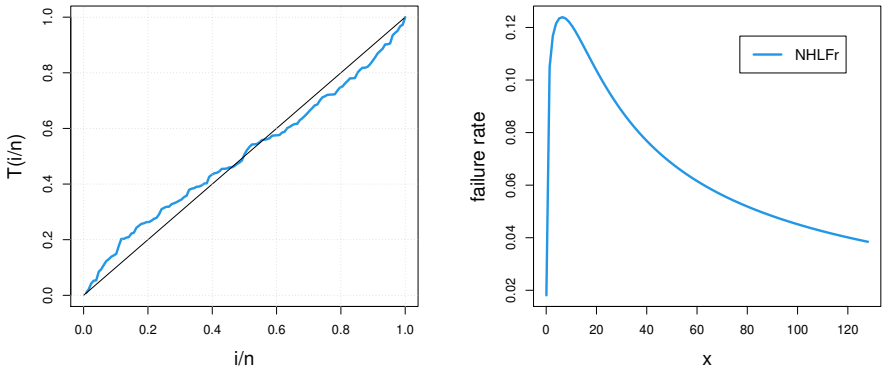

Figure 10. TTT and estimated hazard rate plots for the cancer data set

Table 7. Estimates, the corresponding SEs (given in parentheses) and the goodness of fit measures of the model parameter for the cancer data

Model	Estimates				AICs	BICs	CvM	AD	PV(K-S)
NHLFr	3.084	0.224	61.172	(–)	827.807	836.363	0.046	0.308	0.877
(a, b, λ)	(0.623)	(0.065)	(8.095)						
BFr	0.739	62.050	0.269	8.036	831.823	843.234	0.060	0.413	0.852
(α, β, a, b)	(0.420)	(47.844)	(0.076)	(2.169)					
EGFr	39.797	0.769	7.353	0.294	832.926	844.334	0.068	0.473	0.829
(α, β, a, b)	(24.294)	(0.391)	(1.770)	(0.073)					
HLFr	83.554	6.458	0.217	(–)	827.969	836.418	0.051	0.317	0.869
(λ, a, b)	(10.822)	(1.270)	(0.065)						
EFr	167.967	7.920	0.201	(–)	828.724	837.280	0.052	0.358	0.807
(θ, a, b)	(83.203)	(1.070)	(0.041)						
ZBGaFr	10.081	0.002	2.144	(–)	879.99	888.555	0.556	3.461	0.016
(θ, a, b)	(0.335)	(0.000)	(0.120)						
TLFr	0.769	4.128	0.617	(–)	868.189	876.745	0.485	2.888	0.072
(θ, a, b)	(0.450)	(1.968)	(0.053)						
MoFr	19.726	0.431	1.253	(–)	853.679	862.235	0.215	1.442	0.178
(α, a, b)	(10.174)	(0.167)	(0.097)						
Fr	2.432	0.752	(–)	(–)	892.002	897.706	0.744	4.546	0.013
(a, b)	(0.219)	(0.042)							

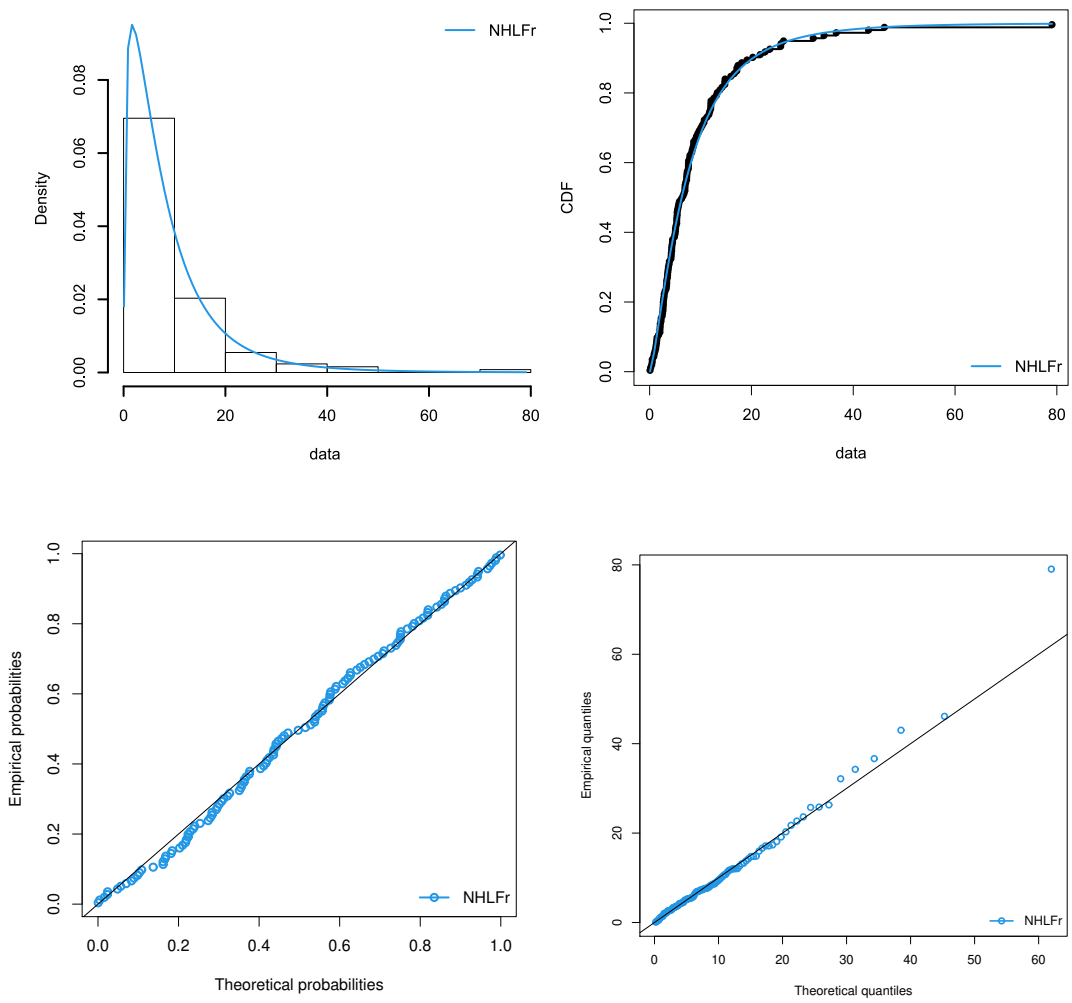

Figure 11. Estimated density, cdf, PP-plot, and QQ-plot for the cancer data

Table 8. The confidence intervals of cancer data set

CI	a	b	λ
95%	[1.863 4.306]	[0.097 0.351]	[45.306 77.038]
99%	[1.477 4.691]	[0.056 0.392]	[40.287 82.057]

The variance-covariance matrices of the MLEs of the NHLFr distribution for cancer data is

$$\begin{pmatrix} 0.38801706 & -0.037248478 & 9.020134 \\ -0.03724848 & 0.004203568 & -5.061557 \\ 9.02013423 & -5.061556821 & 15.029424 \end{pmatrix}$$

3.6.2. Covid 1 data

Recently, Marzouki et al. [2] studied the daily confirmed cases of COVID-19 in Pakistan from March to April 2020 (36 days). In order to maintain transparency, the data are: 2, 2, 3, 4, 26, 24, 25, 19, 4, 40, 87, 172, 38, 105, 155, 35, 264, 69, 283, 68, 199, 120, 67, 36, 102, 96, 90, 181, 190, 228, 111, 163, 204, 192, 627, 663. The descriptive statistics related to this data are given in Table 9. Specifically, in Figure 12, the TTT plot is indicative of a decreasing hrf along with the estimated hrf of NHLFr. The MLEs (with SEs in parenthesis), AICs, BICs, AD, CvM and PV(K-S) are listed in Table 10 while the CI

are given in Table 11. By far, GoF metrics indicate that the NHLFr model is superior to its competitors. The estimated pdf, cdf, PP and Q-Q plots are displayed in Figure 13 of the NHLFr model.

Table 9. The descriptive statistics of the Covid 1 data

Sample size	Mean	Median	SD	Minimum	Maximum	Skewness	Kurtosis
36	130.39	93	149.70	2	663	2.27	5.46

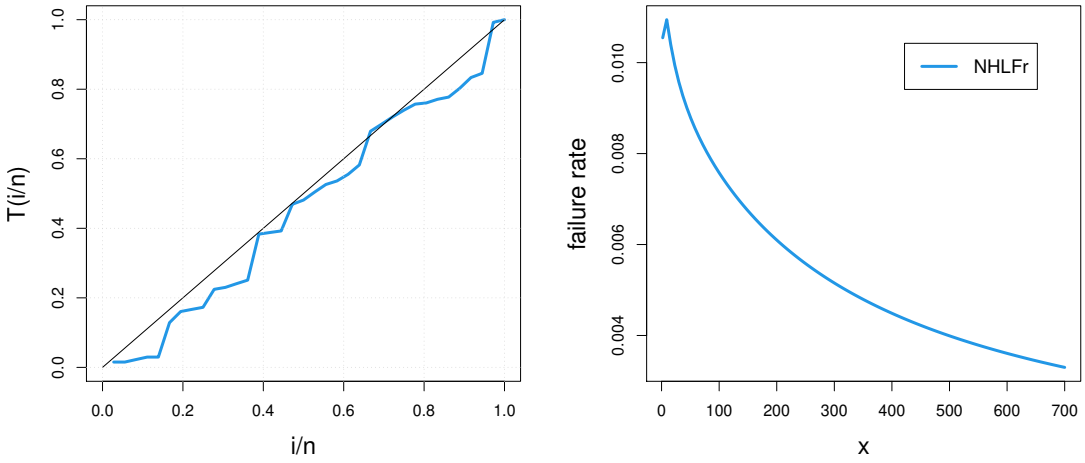

Figure 12. TTT and estimated hazard rate plots for the Covid 1 data

Table 10. Estimates, the respective SEs (given in parentheses) and the goodness of fit statistical measures of the model parameters for the Covid 1 data

Model	Estimates				AIC	BIC	CvM	AD	PV(K-S)
NHLFr	4.396	0.161	83.735	(–)	428.632	433.382	0.094	0.662	0.78
(a, b, λ)	(0.723)	(0.048)	(16.962)						
BFr	0.262	76.639	0.294	25.207	430.891	437.225	0.113	0.773	0.49
(α, β, a, b)	(0.202)	(24.821)	(0.102)	(17.063)					
EGFr	119.959	0.301	22.186	0.272	430.544	436.878	0.105	0.726	0.54
(α, β, a, b)	(88.936)	(0.191)	(11.611)	(0.102)					
HLFr	8.843	0.161	91.797	(–)	429.869	434.619	0.105	0.693	0.72
(λ, a, b)	(1.408)	(0.049)	(24.633)						
EFr	76.638	9.755	0.173	(–)	430.964	435.714	0.138	0.931	0.51
(θ, a, b)	(44.282)	(1.331)	(0.041)						
ZBGaFr	15.330	0.003	2.276	(–)	440.435	445.185	0.314	1.970	0.14
(θ, a, b)	(1.853)	(0.002)	(0.377)						
TLFr	0.407	17.291	0.502	(–)	441.393	446.143	0.326	2.039	0.15
(θ, a, b)	(0.216)	(7.654)	(0.083)						
MoFr	150.492	1.149	1.200	(–)	433.552	438.303	0.164	1.093	0.75
(α, a, b)	(87.382)	(0.412)	(0.178)						
Fr	7.145	0.593	(–)	(–)	445.051	448.218	0.418	2.540	0.14
(a, b)	(1.702)	(0.070)							

The variance-covariance matrix of the MLEs of the NHLFr distribution for Covid 1 data is

$$\begin{pmatrix} 0.37670404 & -0.00392489 & -2.600704 \\ -0.00392489 & 0.001313201 & 35.891992 \\ -2.60070362 & 35.89199242 & 56.790262 \end{pmatrix}$$

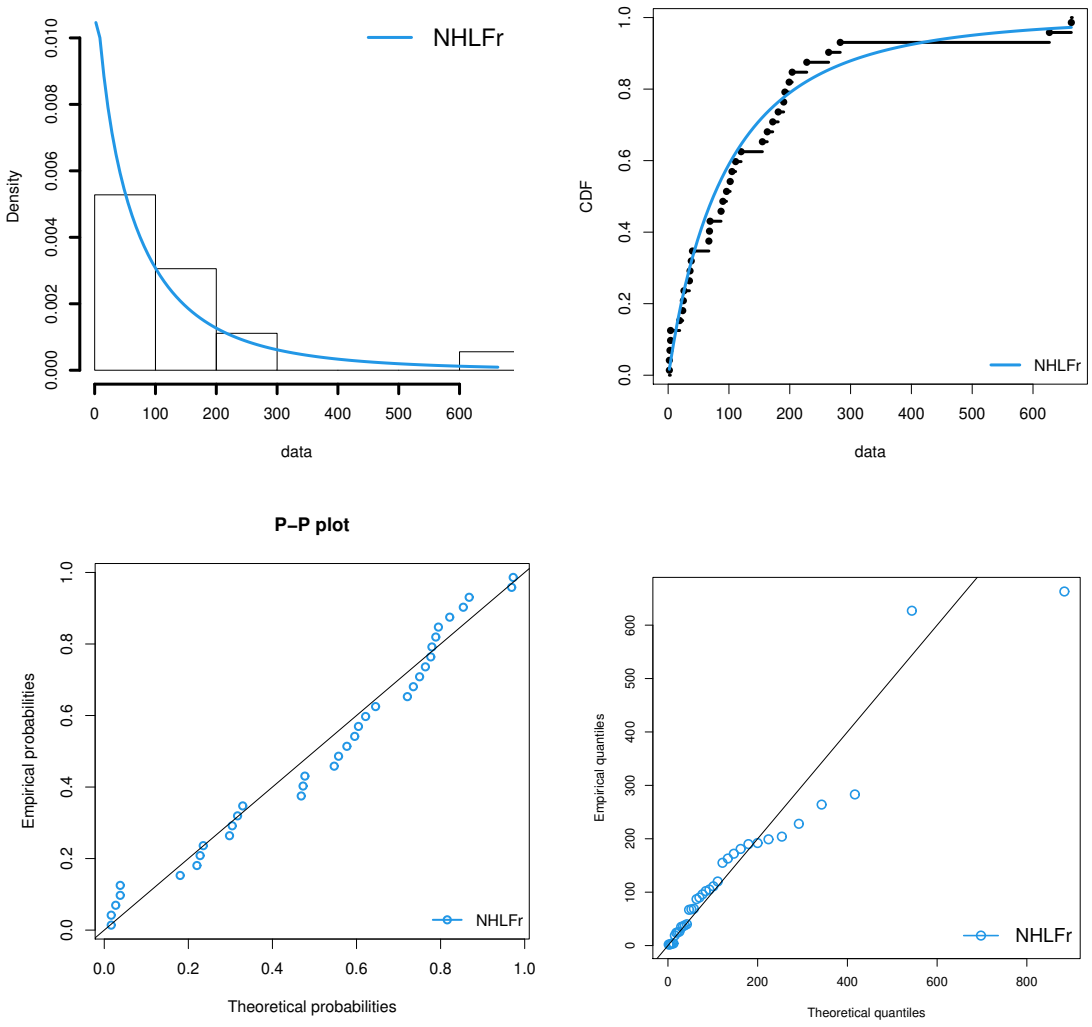

Figure 13. Estimated density, cdf, PP-plot, and QQ-plot for the Covid 1 data

Table 11. The confidence intervals of the Covid 1 data

CI	a	b	λ
95%	[2.979 5.813]	[0.067 0.255]	[50.489 116.981]
99%	[2.538 6.254]	[0.038 0.284]	[40.143 127.327]

3.6.3. Covid 2 data

As of October 27, 2021, the World Health Organization (WHO) received reports of 244,385,444 confirmed cases of COVID-19, with 4,961,489 deaths. A total of 6,697,607,393 vaccine doses indeed were transmitted as of October 24, 2021. This resulted in a decline in the daily number of reported deaths, globally. The third data set incorporates the worldwide deaths reported in the last 24 hours. The countries who reported no deaths were excluded. The data was accessed on October 26, 2021 and is specifically given as: 356, 187, 38, 110, 6, 232, 38, 140, 3, 3, 35, 30, 128, 35, 93, 9, 734, 149, 92, 33, 6, 32, 66, 7, 8, 16, 523, 6, 1, 5, 9, 62, 5, 34, 9, 9, 65, 14, 44, 11, 15, 1, 54, 6, 43, 6, 94, 15, 243, 2, 21, 3, 22, 1, 18, 8, 30, 10, 32, 2, 19, 15, 22, 38, 48, 57, 3, 32, 28, 4, 27, 1, 11, 6, 8, 3, 6, 3, 14, 1, 11, 3, 6, 4, 3, 4, 1, 2, 9, 11, 4, 4, 3, 3, 13, 1, 1, 6, 7, 1, 1, 4, 1,10. Ukraine reported the highest number of deaths in a day. Further,

the descriptive statistics related to Covid 2 data are given in Table 12. In particular, the decreasing TTT plot is well-matched with the estimated hrf of NHLFr in Figure 14. The MLEs (with SEs in parenthesis), AICs, BICs, AD, CvM and PV(K-S), are listed in Table 13 while the CI are given in Table 14. The GoF measures enforce the superiority of NHLFr model over its competitors. Graphically, the estimated pdf, cdf, PP and Q-Q plots are displayed in Figure 15 of the NHLFr model.

Table 12. The descriptive statistics of the Covid 2 data

Sample size	Mean	Median	SD	Minimum	Maximum	Skewness	Kurtosis
104	94.64	10	538.86	1	734	9.61	93.08

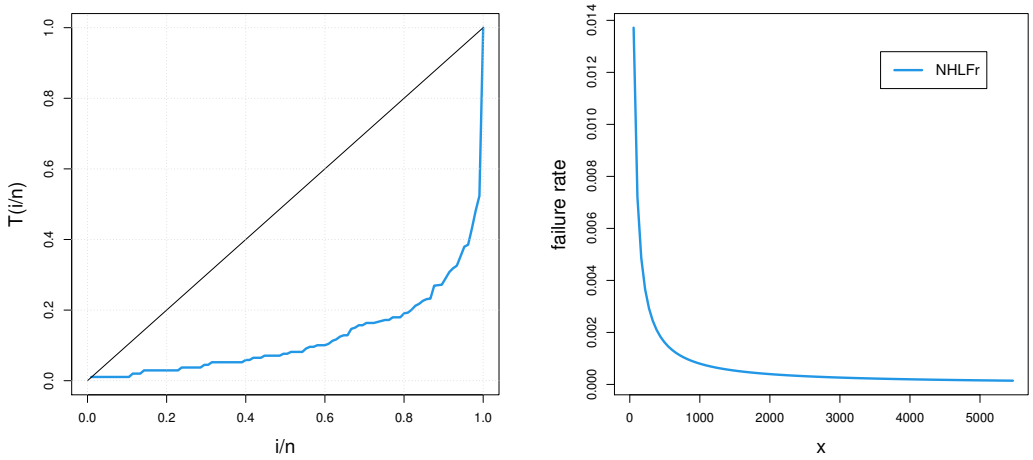

Figure 14. TTT and estimated hazard rate plots for the Covid 2 data

Table 13. Estimates along with the respective SEs (given in parentheses) of the model parameters for the Covid 2 data and the goodness of fit statistical measures

Model	Estimates				AICs	BICs	CvM	AD	PV(K-S)
NHLFr	1.488	0.629	1.224	(–)	936.506	944.46	0.526	0.053	0.692
(a, b, λ)	(0.204)	(0.174)	(0.521)						
BFr	0.109	1.725	0.634	31.791	937.733	948.349	0.558	0.058	0.671
(α, β, a, b)	(0.176)	(0.764)	(0.101)	(5.098)					
EGFr	3.222	7.600	1.295	0.304	938.450	949.116	0.536	0.059	0.667
(α, β, a, b)	(1.074)	(5.135)	(0.264)	(0.098)					
HLFr	1.143	2.883	0.760	(–)	943.709	945.671	0.591	0.056	0.661
(λ, a, b)	(0.614)	(0.505)	(0.264)						
EFr	3.954	0.523	1.831	(–)	938.514	945.538	0.685	0.067	0.680
(θ, a, b)	(0.536)	(0.153)	(1.052)						
ZBGaFr	7.293	0.043	1.631	(–)	953.546	958.507	0.562	0.058	0.637
(θ, a, b)	(4.273)	(0.128)	(0.537)						
TLFr	0.154	22.460	0.617	(–)	937.837	945.120	0.569	0.057	0.686
(θ, a, b)	(0.088)	(14.567)	(0.117)						
MoFr	3.188	2.301	0.896	(–)	939.382	948.601	0.602	0.060	0.665
(α, a, b)	(2.363)	(0.864)	(0.121)						
Fr	3.552	0.717	(–)	(–)	938.565	945.873	0.801	0.080	0.577
(a, b)	(0.411)	(0.054)							

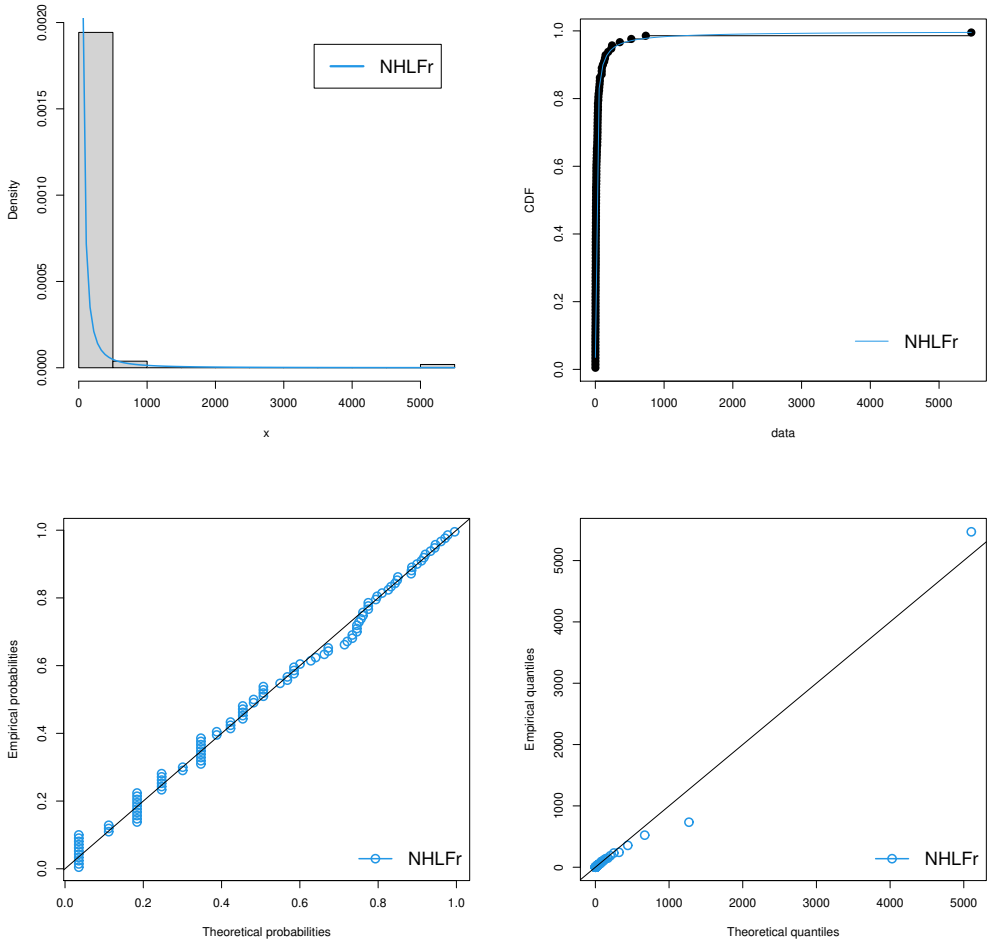

Figure 15. Estimated (a) density (b) cdf (c) PP-plot, and (d) QQ-plot for the Covid 2 data

Table 14. The confidence intervals of the Covid 2 data

CI	a	b	λ
95%	[0.288 0.970]	[1.088 1.888]	[0.203 2.245]
99%	[0.179 1.078]	[0.962 2.014]	[0 2.568]

The variance-covariance matrices of the MLEs of the NHLFr distribution for Covid 2 data is

$$\begin{pmatrix} 0.04161658 & -0.01236045 & 0.05468762 \\ -0.01236045 & 0.03033496 & -0.08736272 \\ 0.05468762 & -0.08736272 & 0.27149359 \end{pmatrix}$$

4. Concluding remarks

The NHLG class of distribution is presented and studied with some mathematical properties such as ordinary and incomplete moments, mean deviations and generating functions. The model parameters are estimated using the greatest likelihood method. To ensure that the projections have asymptotic characteristics, simulations are run. Three applications to real data sets are offered to highlight the potential of the proposed models. The presented models are considered an effective tool in a range of sectors, particularly in bioinformatics.

Acknowledgement

The authors are grateful to the lead Editor, and anonymous reviewers for their valuable comments and suggestions made on the previous draft of this manuscript.

References

[1] Abbas, S., Taqi, S. A., Mustafa, F., Murtaza, M., and Shahbaz, M. Q. Topp-Leone inverse Weibull distribution: Theory and application. *European Journal of Pure and Applied Mathematics 10*, 5 (2017), 1005–1022.

[2] Al-Marzouki, S., Jamal, F., Chesneau, C., and Elgarhy, M. Topp-Leone odd Fréchet generated family of distributions with applications to COVID-19 data sets. *Computer Modeling in Engineering & Sciences 125*, 1 (2020), 437–458.

[3] Alzaatreh, A., Lee, C., and Famoye F. A new method for generating families of continuous distributions. *Metron 71*, 1 (2013), 63–79.

[4] Barreto-Souza, W., Cordeiro, G. M., and Simas, A. B. Some results for beta Fréchet distribution. *Communications in Statistics - Theory and Methods 40*, 5 (2011), 798–811.

[5] Cordeiro, G. M., Alizadeh, M., and Diniz Marinho, P. R. The type I half-logistic family of distributions. *Journal of Statistical Computation and Simulation 86*, 4 (2016), 707–728.

[6] Cordeiro, G. M., Ortega, E. M. M., and da Cunha, D. C. C. The exponentiated generalized class of distributions. *Journal of Data Science 11*, 1 (2013), 1–27.

[7] da Silva, R. V., de Andrade, T. A. N., Maciel, D. B. M., Campos, R. P. S., and Cordeiro, G. M. A new lifetime model: The gamma extended Fréchet distribution. *Journal of Statistical Theory and Applications 12*, 1 (2013), 39–54.

[8] Fréchet, R. M. On the probability law of maximum deviation. *Annales de la Société Polonaise de Mathématique 6* (1927), 93–116, (in French).

[9] Granzotto, D. C. T., Louzada, F., and Balakrishnan, N. Cubic rank transmuted distributions: inferential issues and applications. *Simulation 87*, 14 (2017), 2760–2778.

[10] Gupta, R. D., and Kundu, D. Exponentiated exponential family: An alternative to gamma and Weibull distributions. *Biometrical Journal 43*, 1 (2001), 117–130.

[11] Kotz, S., and Nadarajah, S. Kotz-Type Distribution. In *Encyclopedia of Statistical Sciences*, N. Balakrishnan, N. L. Johnson and S. Kotz, Eds., 2nd. ed. John Wiley & Sons, Ltd, 2006.

[12] Krishna, E., Jose, K. K., and Ristić, M. M. Applications of Marshall–Olkin Fréchet distribution. *Communications in Statistics - Simulation and Computation 42*, 1 (2013), 76–89.

[13] Lee E. T., and Wang J. W. *Statistical Methods for Survival Data Analysis*. Vol. 476. John Wiley & Sons, 2003.

[14] Lehmann, E. L. The power of rank tests. *Annals of Mathematical Statistics 24*, 1 (1953), 23–43.

[15] Marshall, A. W., and Olkin, I. A new method for adding parameters to a family of distributions with application to the exponential and Weibull families. *Biometrika 84*, 3 (1997), 641–652.

[16] Mudholker, G. S., and Srivastava, D. K. Exponentiated Weibull family for analyzing bathtub failure-rate data. *IEEE Transactions of Reliability 42*, 2 (1993), 299–302.

[17] Nadarajah, S., and Gupta, A. K. The beta Fréchet distribution. *Far East Journal of theoretical Statistics 14*, 1 (2004), 15–24.

[18] Nadarajah, S., and Kotz, S. The exponentiated type distributions. *Acta Applicandae Mathematica 92*, 2 (2006), 99–111.

[19] Shaw, W. T., and Buckley, I. R. C. The alchemy of probability distributions: beyond Gram-Charlier expansions, and a skew-kurtotic-normal distribution from a rank transmutation map, 2009. Available from https://arxiv.org/abs/0901.0434.

[20] Tahir, M. H., Hussain, M. A., and Cordeiro, G. C. A new flexible generalized family for constructing many families of distributions. *Journal of Applied Statistics 23* (2021), 1615–1635.